

Fabrication of gold nanorods-doped, bovine serum albumin microstructures via multiphoton excited photochemistry

Chi-Hsiang Lien,¹ Wen-Shuo Kuo,¹ Keng-Chi Cho,² Chun-Yu Lin,¹ Yuan-Deng Su,¹ Lynn L. H. Huang,³ Paul J. Campagnola,⁴ Chen Yuan Dong,^{5,7} and Shean-Jen Chen^{1,6,*}

¹Department of Engineering Science, National Cheng Kung University, Tainan 701, Taiwan

²Institute of Electro-Optical Science and Engineering, National Cheng Kung University, Tainan 701, Taiwan

³Institute of Biotechnology, National Cheng Kung University, Tainan 701, Taiwan

⁴Department of Biomedical Engineering, University of Wisconsin-Madison, Madison, Wisconsin 53706, USA

⁵Department of Physics, National Taiwan University, Taipei 106, Taiwan

⁶Advanced Optoelectronic Technology Center, National Cheng Kung University, Tainan 701, Taiwan

⁷cydong@phys.ntu.edu.tw

*sheanjen@mail.ncku.edu.tw

Abstract: In this study, three-dimensional (3D) crosslinked bovine serum albumin (BSA) microstructures containing gold nanorods (AuNRs) were fabricated via multiphoton excited photochemistry using Rose Bengal (RB) as the photoactivator. To retain AuNRs in the 3D crosslinked BSA microstructures, the laser wavelength was chosen for two-photon RB absorption for improved two-photon crosslinking efficiency, but not for enhancing the longitudinal plasmon resonance of AuNRs which may result in photothermal damage of AuNRs. Furthermore, with two-photon excitation of RB via AuNRs plasmonics, the laser power can be reduced by about 30%. As a result, 3D BSA microstructures containing AuNRs can be successfully fabricated. The AuNRs-doped BSA microstructures can be applied in biomedical scaffolds with plasmonic properties such as two-photon luminescence imaging and photothermal therapy.

© 2011 Optical Society of America

OCIS codes: (120.4610) Optical fabrication; (190.4180) Multiphoton processes; (240.6680) Surface plasmons.

References and links

1. C. R. Lambert, I. E. Kochevar, and R. W. Redmond, "Differential reactivity of upper triplet states produces wavelength-dependent two-photon photosensitization using Rose Bengal," *J. Phys. Chem. B* **103**(18), 3737–3741 (1999).
2. J. D. Pitts, P. J. Campagnola, G. A. Epling, and S. L. Goodman, "Submicron multiphoton free-form fabrication of proteins and polymers: studies of reaction efficiencies and applications in sustained release," *Macromolecules* **33**(5), 1514–1523 (2000).
3. S. Kawata, H. B. Sun, T. Tanaka, and K. Takada, "Finer features for functional microdevices," *Nature* **412**(6848), 697–698 (2001).
4. P. Galajda and P. Ormos, "Complex micromachines produced and driven by light," *Appl. Phys. Lett.* **78**(2), 249–251 (2001).
5. T. Watanabe, M. Akiyama, K. Totani, S. M. Kuebler, F. Stellacci, W. Wenseleers, K. Braun, S. R. Marder, and J. W. Perry, "Photoresponsive hydrogel microstructure fabricated by two-photon initiated Polymerization," *Adv. Funct. Mater.* **12**(9), 611–614 (2002).
6. Z. B. Sun, X. Z. Dong, W. Q. Chen, S. Nakanishi, M. Duan, and S. Kawata, "Multicolor polymer nanocomposites: in situ synthesis and fabrication of 3D microstructures," *Adv. Mater. (Deerfield Beach Fla.)* **20**(5), 914–919 (2008).
7. M. A. Swartz, "Signaling in morphogenesis: transport cues in morphogenesis," *Curr. Opin. Biotechnol.* **14**(5), 547–550 (2003).
8. L. Liaw, M. P. Skinner, E. W. Raines, R. Ross, D. A. Cheresh, S. M. Schwartz, and C. M. Giachelli, "The adhesive and migratory effects of osteopontin are mediated via distinct cell surface integrins. Role of alpha v beta 3 in smooth muscle cell migration to osteopontin in vitro," *J. Clin. Invest.* **95**(2), 713–724 (1995).

9. S. Basu, L. P. Cunningham, G. D. Pins, K. A. Bush, R. Taboada, A. R. Howell, J. Wang, and P. J. Campagnola, "Multi-photon excited fabrication of collagen matrices crosslinked by a modified benzophenone dimer: Bioactivity and enzymatic degradation," *Biomacromolecules* **6**(3), 1465–1474 (2005).
10. G. D. Pins, K. A. Bush, L. P. Cunningham, and P. J. Campagnola, "Multiphoton excited fabricated nano and micropatterned extracellular matrix proteins direct cellular morphology," *J. Biomed. Mater. Res.* **78A**(1), 194–204 (2006).
11. R. T. Hill, J. L. Lyon, R. Allen, K. J. Stevenson, and J. B. Shear, "Microfabrication of three-dimensional bioelectronic architectures," *J. Am. Chem. Soc.* **127**(30), 10707–10711 (2005).
12. W. S. Kuo, C. N. Chang, Y. T. Chang, M. H. Yang, Y. H. Chien, S. J. Chen, and C. S. Yeh, "Gold nanorods in photodynamic therapy, as hyperthermia agents, and in near-infrared optical imaging," *Angew. Chem. Int. Ed. Engl.* **49**(15), 2711–2715 (2010).
13. W. S. Kuo, C. M. Wu, Z. S. Yang, S. Y. Chen, C. Y. Chen, C. C. Huang, W. M. Li, C. K. Sun, and C. S. Yeh, "Biocompatible bacteria@Au composites for application in the photothermal destruction of cancer cells," *Chem. Commun. (Camb.)* **37**(37), 4430–4432 (2008).
14. W. S. Kuo, C. N. Chang, Y. T. Chang, and C. S. Yeh, "Antimicrobial gold nanorods with dual-modality photodynamic inactivation and hyperthermia," *Chem. Commun. (Camb.)* **32**(32), 4853–4855 (2009).
15. J. Nappa, G. Revillod, J. P. Abid, I. Russier-Antoine, C. Jonin, E. Benichou, H. H. Girault, and P. F. Brevet, "Hyper-Rayleigh scattering of gold nanorods and their relationship with linear assemblies of gold nanospheres," *Faraday Discuss.* **125**, 145–156 (2004).
16. A. K. Singh, D. Senapati, S. Wang, J. Griffin, A. Neely, P. Candice, K. M. Naylor, B. Varisli, J. R. Kalluri, and P. C. Ray, "Gold nanorod based selective identification of *Escherichia coli* bacteria using two-photon Rayleigh scattering spectroscopy," *ACS Nano* **3**(7), 1906–1912 (2009).
17. Q. Liao, C. Mu, D. S. Xu, X. C. Ai, J. N. Yao, and J. P. Zhang, "Gold nanorod arrays with good reproducibility for high-performance surface-enhanced Raman scattering," *Langmuir* **25**(8), 4708–4714 (2009).
18. A. L. Oldenburg, M. N. Hansen, D. A. Zweifel, A. Wei, and S. A. Boppert, "Plasmon-resonant gold nanorods as low backscattering albedo contrast agents for optical coherence tomography," *Opt. Express* **14**(15), 6724–6738 (2006).
19. N. J. Durr, T. Larson, D. K. Smith, B. A. Korgel, K. Sokolov, and A. Ben-Yakar, "Two-photon luminescence imaging of cancer cells using molecularly targeted gold nanorods," *Nano Lett.* **7**(4), 941–945 (2007).
20. Y. Zhang, K. Aslan, M. J. R. Previte, and C. D. Geddes, "Plasmonic engineering of singlet oxygen generation," *Proc. Natl. Acad. Sci. U.S.A.* **105**(6), 1798–1802 (2008).
21. K. Aslan, S. N. Malyn, and C. D. Geddes, "Metal-enhanced fluorescence from gold surfaces: angular dependent emission," *J. Fluoresc.* **17**(1), 7–13 (2006).
22. W. S. Kuo, C.-H. Lien, K.-C. Cho, C.-Y. Chang, C.-Y. Lin, L. L. H. Huang, P. J. Campagnola, C.-Y. Dong, and S.-J. Chen, "Multiphoton fabrication of freeform polymer microstructures with gold nanorods," *Opt. Express* **18**(26), 27550–27559 (2010).
23. C. Xu and W. W. Webb, "Measurement of two-photon excitation cross sections of molecular fluorophores with data from 690 to 1050 nm," *J. Opt. Soc. Am. B* **13**(3), 481–491 (1996).
24. D. C. Neckers, "Rose Bengal," *J. Photochem. Photobiol., A* **47**(1), 1–29 (1989).
25. S. Link, C. Burda, B. Nikoobakht, and M. A. El-Sayed, "Laser-induced shape changes of colloidal gold nanorods using femtosecond and nanosecond laser pulses," *J. Phys. Chem.* **104**(26), 6152–6163 (2000).

1. Introduction

Photopolymerization or photocrosslinking is a process which uses a combination of light with low molecular weight photoinitiators or photoactivators to trigger the respective reactions of polymerization or crosslinking reaction [1,2]. Moreover, in order to fabricate polymer-based microstructure in three-dimensions (3D), multiphoton excited (MPE) photochemistry is the preferred technique. Since multiphoton absorption can be confined to the focal volume of a high numerical aperture (NA) objective, fabricated structures with the desired 3D submicron features can be created with a 3D scanning system [3,4]. This approach not only allows the creation of structures that cannot be constructed by conventional single-photon lithography, but also provides greater spatial resolution than other 3D microfabrication techniques. Therefore, multiphoton polymerization and crosslinking have attracted widespread interest due to its potential use in fabricating intrinsic 3D microstructures with sub-diffraction limited spatial resolution [4]. The utilization of short pulse width and tight focusing are critical for inducing sufficient extent of two-photon absorption (TPA) and for achieving high precision fabrication. For the work presented hereafter, a femtosecond (fs) titanium-sapphire (ti-sa) laser was used as the excitation source. Previously, fs 3D microfabrication has been demonstrated in polymerized resin- [3,5,6] and protein-crosslinked [2] structures. The fabricated protein microstructures have potential in many biological applications. It is now

well-appreciated that spatial concentration gradients of bioactive molecules such laminin and fibronectin in the extracellular matrix (ECM) play important roles in several areas of cell biology, including morphogenesis, wound healing, and metastasis [7,8]. Our previous efforts using the MPE photochemistry technology have been directed at fabricating and characterizing scaffolds from several ECM proteins and the concomitant cell response [9,10].

Recently, to incorporate electrical monitoring and stimulation in microbiological systems, 3D protein structures with conductive metallic material were developed [11]. The metallic biomaterial approach may offer electrical scaffolds created with electrochemical architectures, nanoelectronic components, and cellular interfaces. Among the developed metallic nanomaterials for biomedical applications, gold nanoparticles (AuNPs) are particularly attractive due to their biocompatibility ability to create protein structures that are electrically conductive. In order to create these structures in 3D using optical excitation, near infrared (NIR) light is preferred due to its optimal tissue transmission from reduced scattering and energy absorption. As a result, maximum irradiation penetration through tissue and minimization of the auto-fluorescence of non-target tissue can be achieved [12]. Therefore, there have been efforts aiming at shifting the surface plasmon resonance (SPR) of AuNPs into the NIR region for potential biological applications [13,14]. Numerous NIR-absorbing, Au-based bionanomaterials have been developed. Specifically, Au nanorods (AuNRs) with different aspect ratios and corresponding longitudinal plasmon resonance in the 700 to 1000 nm fall within the spectral range of the fs Ti:sapphire laser. AuNRs designed with these properties have been applied in localized SPR light scattering [15], Rayleigh elastic scattering [16], surface-enhanced Raman inelastic scattering [17], optical coherent tomography scattering [18], two-photon luminescence (TPL) imaging [19], and photothermal therapy [12–14]. In addition, the surface plasmonic engineering of AuNPs has received significant attention [20,21]. For the interactions of fluorophores with AuNPs (AuNRs), nonradiative energy transfer takes place from excited distal fluorophores to the surface plasmon electrons on non-continuous films. In return, this process results in the phenomenon of metal-enhanced fluorescence. The use of AuNRs results in increased photostability for photoinitiators, enhance intersystem crossing, and increase triplet yield of the photoinitiators. Based on these phenomena, AuNRs could be utilized to enhance nonlinear photopolymerization and photocrosslinking in the NIR region.

While AuNRs have found wide biomedical applications, the use of AuNRs in 3D protein microfabrication has been rare. Due to the fact that AuNRs-doped protein microstructures exhibit unique electrical, optical, and mechanical properties, and photocrosslinking enhancement, in this work, we explored these properties for protein microfabrication. Specifically, two-photon crosslinking (TPC) using bovine serum albumin (BSA) as a reactive protein, Rose Bengal (RB) as a photoactivator, Tween 20 as a surfactant for AuNRs, and cetyltrimethylammonium bromide (CTAB)-coated AuNRs were used to direct the 3D assembly of BSA microstructures. BSA is a common blood plasma protein, which facilitates the distribution of various molecular ligands to specific targets, and has been used in protein microfabrication [2]. Herein, we present the first example of 3D crosslinked BSA microstructures uniformly containing two-photon excitable AuNRs by using a threshold laser power without damage to the AuNRs. In order to retain AuNRs in the 3D crosslinked BSA microstructures, an optimal laser wavelength was first chosen for TPA of RB for improved TPC efficiency, but not for enhancing the longitudinal plasmon resonance of AuNRs which may result in photothermal damage of AuNRs. With the plasmonic engineering of AuNRs for two-photon excitation of RB, the laser power can be significantly reduced. Moreover, due to the fact that most nanoparticles are difficult to disperse in high concentration protein solution, we improved the fabrication efficiency and the uniformity of embedded AuNR by mixing a suitable content with BSA, RB, and CTAB-coated AuNRs with sufficient Tween 20. This approach is expected to enable the fabrication of 3D BSA microstructures while retaining the

AuNRs. With TPL imaging, we will also demonstrate that the AuNRs-doped BSA microstructures can be used as 3D scaffolds.

2. Sample preparation and microfabrication procedure

2.1. Sample preparation

Hydrogen tetrachloroaurate (III) hydrate (HAuCl_4) was purchased from Alfa Aesar Co. (Ward Hill, MA, USA). CTAB, ascorbic acid, silver nitrate, sodium tetrahydroborate, BSA, xanthene dye (RB), and Tween 20 were purchased from Sigma-Aldrich Co. (St. Louis, MO, USA). All chemicals and reagents were of the analytical grade. The AuNRs were synthesized using the seedless growth method [13,14]. The mean length and width of the AuNRs were approximately 50.2 nm and 11.2 nm, respectively, and their aspect ratio (length divided by width) was about 4.5. Electron micrographs of the AuNRs were acquired by the use of transmission electron microscopes (TEM) (Jeol 1200, at 80 kV; Jeol 3010, at 300 kV; and Philips CM-200, at 200 kV, Japan) and a scanning electron microscope (SEM) (Jeol 7000). BSA was utilized as the reactive protein. The fabrication solution is consisted of 5.0 mM RB solution (photoactivator) and 10% (v/v) Tween 20 (surfactant) mixed into the BSA protein solution.

AuNRs with CTAB coating were synthesized using the seedless growth method. Due to the presence of CTAB, the surface charge of the AuNRs revealed a zeta potential of approximately 39.2 mV by using a spectrometer (Manern Nano-ZS90, UK). As shown in Fig. 1(a), measurement using a UV/Vis absorption spectrometer (Agilent 8453, USA) shows that AuNRs exhibit two plasmon resonances. A transverse plasmon resonance (about 520 nm in water) and a longitudinal plasmon resonance (about 835 nm in water; 850 nm in the fabrication solution) were found. On the other hand, the absorption spectrum of RB exhibited one main peak at around 550 nm (Fig. 1(b)), while a similar band appeared in the RB-containing fabrication solution with the AuNRs and BSA (Fig. 1(a)). Shown in Fig. 1(b) are the absorption spectra of BSA, aqueous RB, and Tween 20.

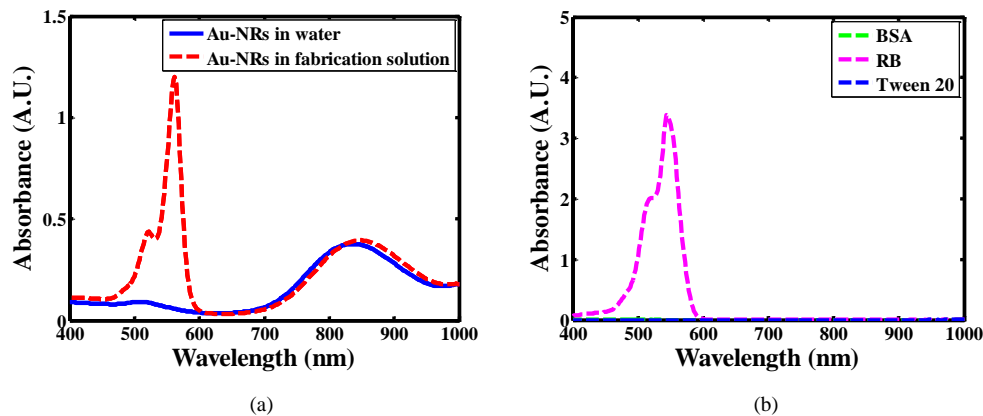


Fig. 1. (a) UV/Vis spectra of AuNRs in water and fabrication solution with 50 mg/ml BSA. (b) UV/Vis spectra of BSA, aqueous RB, and Tween 20.

2.2. Microfabrication instrument and the design of freeform structures

The multiphoton fabrication instrument/microscope has been described in detail previously [22]. Briefly, key components of our instrument include a femtosecond laser (Tsunami, Spectra-Physics, USA), an inverted optical microscope (Axiovert 200, Zeiss, Germany), galvanometer x - y scanner (6215H, Cambridge, USA), a triple-axis sample positioning stage (ProScanTMII, Prior, UK), a z -axis piezoelectric nano-positioning stage (Nano-F100, Mad City Labs, USA), an acousto-optic modulator (AOM) (23080-x-1.06-LTD, Neos, USA),

photomultiplier tubes (H5783P, Hamamatsu, Japan), and a data acquisition (DAQ) card with a field-programmable gate array (FPGA) module (PCI-7831R, National Instruments, USA). The FPGA module was designed to perform a number of simultaneous tasks including control of the galvanometer scanner and the *z*-axis piezoelectric stage for positioning of the 3D focal spot; modulating the AOM for rapid on/off switching of the laser and pulse selection; and processing of the single photon counting signals.

The real-time FPGA DAQ card based on our custom LabVIEW program can synchronously control the instrument through interfaces constructed in-house. A digital I/O via a voltage converter is connected to the AOM for fast on/off laser control. A rate of up to 9 MHz can be achieved. In addition to nonlinear optical imaging capabilities, CAD software such as AutoCAD, Pro/E, and Solidworks can be used to design 3D structures for microfabrication. To transform 3D structures into two-dimensional (2D) processing patterns, our designed transformation program was used to convert the 3D structures into sequential 2D bitmap files. The 2D bitmap files were downloaded into the FPGA module as laser processing commands. With the use of 3D structure design, we were able to create the desired structures.

2.3. Wavelength selection in femtosecond laser microfabrication

In TPC processing, we can improve the crosslinking efficiency of BSA by adopting the laser wavelength at the maximum TPA of the photoactivator, RB. The TPA (probability) is given by $\delta \times \eta_2$ and expressed as [22,23]

$$\delta\eta_2 \propto \lambda\tau F, \quad (1)$$

where δ is the cross section of TPA of a fluorescence species, η_2 the quantum efficiency of two-photon excited fluorescence (TPEF), λ the excitation wavelength, τ the excitation pulse width at full-width at half maximum, and F the time-averaged TPEF photon count. In TPA spectrum measurement experiment, it was found that the excitation wavelength corresponding to the maximum value of the relative TPA of the RB was between 710 and 720 nm [22]. Therefore, a fabrication laser wavelength of around 715 nm was adopted. Moreover, in order to implement the multiphoton fabrication of 3D crosslinked BSA microstructures with AuNRs, the wavelengths of the two plasmon resonances of the adopted AuNRs should differ significantly from the fabrication wavelength of 715 nm. As shown in Fig. 1(a), the AuNRs with an aspect ratio of approximately 4.5 exhibits two plasmon resonances with transverse plasmon at around 520 nm and longitudinal plasmon at 850 nm in the fabrication solution. Therefore, the AuNRs with a longitudinal plasmon wavelength longer than 800 nm should be good candidates for the TPC process with the RB.

3. Experimental results and discussions

3.1. Freeform crosslinked BSA microstructures

For protein TPC processing, two-photon excited photochemistry drives photoactivators (RB) from ground state into excited vibration state, nonradiative decay to singlet state, and subsequently to long-lived triplet state via intersystem crossing. Then, the active photoactivator efficiently converts triplet oxygen into singlet oxygen [24]. The reactive species then react with a protein molecule, creating a radical that binds to a second protein molecule, and resulting in a covalently crosslinked structure. For 3D microfabrication, the sequential 2D bitmap files sliced from a 3D CAD model were downloaded into the FPGA to control the laser illumination via the AOM. Since TPC is confined to the focal volume, 3D freeform polymer solid structures can be developed. Unreacted solution was then washed out by water three times. Herein, two experimental results demonstrate that freeform crosslinked BSA microstructures fabricated by this approach. To implement multiphoton fabrication of 3D crosslinked BSA microstructures, the power of the 100 fs laser at the repetition rate of 80 MHz must be sufficient to support the MPE photochemistry processing. According to our

experience, the use of NA 1.3 objective and the x -galvanometer scan rate of 1 kHz, the laser power at the TPA wavelength of the photoactivator must be at least one mW in order to implement multiphoton fabrication.

The fabrication solution was confined in a small chamber, which was created by using a 100 μm -thick adhesive tape as a spacer to separate a cover slip and a microscope slide. In our inverted optical microscope-based microfabrication instrument, the BSA TPC processing was started from the top interface of the chamber in order to obtain precise 3D complex microstructures. In this manner, the distortion of focusing laser beam caused by its passing through the partially fabricated microstructure can be avoided. Figure 2(a) shows the 3D rendering of the TPEF image of a high aspect ratio cylinder fabricated from MPE crosslinked BSA, where the height is 60 μm , inner diameter of 60 μm , and wall thickness of 1 μm . Figure 2(b) show a crosslinked BSA microspring with the length of 60 μm , diameter of 10 μm , and pitch of 10 μm . The forms of the fabricated BSA microstructures can be utilized to entrap living cells to perform motility and migration studies.

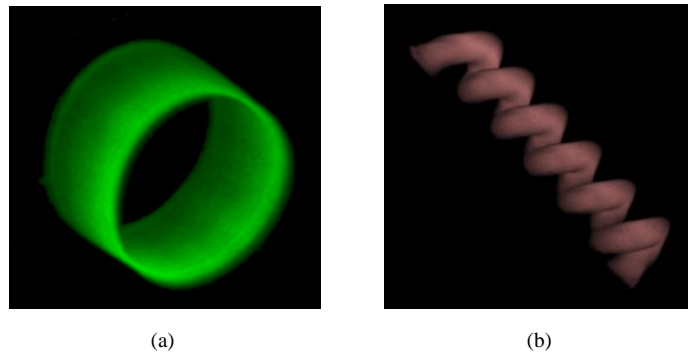


Fig. 2. TPEF images of freeform crosslinked BSA microdevices: (a) Cylinder stained with Texas red and (b) helix stained with RB.

3.2. Plasmon-assisted microfabrication

To fabricate AuNRs-doped BSA microstructures via MPE photochemistry, a content of 50 mg/ml protein (BSA), 5.0 mM photoactivator (RB) with TPA of 715 nm, 10% (v/v) cationic surfactant (Tween 20), and $\sim 10^{13}$ NPs/ml AuNRs with a longitudinal plasmon about 850 nm were mixed as a fabrication solution. RB was chosen due to its higher singlet oxygen quantum yield effective for implementing protein crosslinking processing. Also, Tween 20 was adopted as a surfactant to avoid AuNR aggregation in high concentration protein solution. As mentioned in Sec. 3.1, the power of the 100 fs laser at the repetition rate of 80 MHz must be at least one mW in order to implement the crosslinked BSA fabrication. Compared to two-photon polymerization which uses a resin as a reactive monomer, we found that the laser power of the TPC processing should be higher, preferably doubled [22]. However, AuNRs can be easily reshaped by utilizing the 100 fs laser at the resonance wavelength of the longitudinal plasmon of the AuNRs. Previously, a threshold power for completely melting AuNRs within a linearly polarized (along the longitudinal axis of the AuNRs) laser pulse can be found about 0.96 mW [25]. To retain the AuNRs in crosslinked BSA microstructures, the laser wavelength must be chosen to be 715 nm for RB TPA, not for the longitudinal plasmon resonance of the AuNRs. AuNR damage can be reduced by choosing the AuNRs with the longitudinal plasmon resonance wavelength far away from 715 nm by controlling the aspect ratio of the AuNRs. Therefore, the threshold power of the 715 nm fs laser for avoiding reshaping the AuNRs should be higher than 0.96 mW. In addition, the threshold power for avoiding reshaping the AuNRs can be doubled as the polarization of the laser is changed from linear to circular.

For the plasmonic engineering of AuNRs assisted two-photon excitation of RB, the fabrication laser power of the TPC process can be reduced again in order to alleviate melting

of the AuNRs. Figure 3 shows the bright-field images of attempted fabrication of structures within $10 \times 10 \times 5 \mu\text{m}^3$ in volumes. BSA microstructures filled with (top) and without (bottom) AuNRs with longitudinal plasmon resonance of 850 nm under different fabrication laser powers (0.40 mW to 1.07 mW) are shown. In our experiments, a quarter wave plate (QWP) was inserted after the linear polarizer. The polarization of the laser is changed from linear to circular. The minimum fabrication power of the 100 fs laser to support the BSA TPC processing without the AuNRs is around 0.93 mW (bottom of Fig. 3). In comparison, the minimum fabrication power for the BSA TPC with AuNRs is around 0.67 mW. Examination of Fig. 3 shows that with the use of AuNR, the minimum laser fabrication power can be decreased by about 0.26 mW (0.93 to 0.67 mW). The results demonstrate that the BSA TPC efficiency is enhanced by increasing singlet oxygen generation via AuNRs-photoactivator (RB) interactions. The singlet oxygen yields can be increased due to nonradiative energy transfer coupling from the surface plasmons of noble metal particles, such as AuNPs and Ag particles or AuNRs [20]. It is speculated that the local electric field is enhanced by the longitudinal plasmon resonance of the AuNRs to increase the two-photon excitation of RB. Moreover, the TPL induced from the AuNRs also can achieve BSA crosslinking at the area near the AuNRs by one-photon excitation of RB. Besides, the photothermal effect of the AuNRs is another possible contribution for the observed reduction of fabrication laser power. The localized temperature near the AuNRs can be increased when the AuNRs are excited by the 715 nm fs laser. The reactivity of both RB and BSA can be increased at the elevated temperature. The BSA TPC efficiency may be assisted by the photothermal effect. In this study, an optimal parameter to enhance the BSA TPC efficiency via AuNRs might not be obtained; however, the fabrication laser power below 0.8 mW would result in the minimal damage of AuNR for all of the orientations.

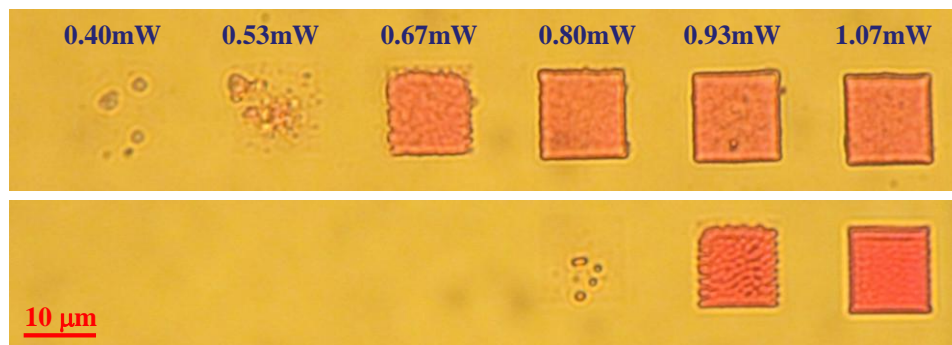


Fig. 3. Bright-field images of crosslinked BSA microstructures at different fabrication laser powers with (top) and without (bottom) AuNRs with longitudinal plasmon resonance of 850 nm assisted. The fabrication laser power varied from 0.40 mW to 1.07 mW (left to right).

3.3. 3D BSA microstructure with AuNRs

TPL from the doped AuNRs can act as contrast agent for the visualization of 3D crosslinked BSA microstructures. However, TPEF from RB and TPL from AuNRs are both induced by fs laser excitation and their spectra may overlap. For AuNRs-doped TPL imaging, the excited wavelength should be chosen to be 850 nm for highly efficient TPL. Figure 4 shows the emission spectra of 5.0 mM RB and $\sim 10^{13}$ NPs/ml AuNR solutions excited by the 100 fs laser at 850 nm and 0.13 mW, respectively. The emission spectra were recorded on a spectrometer (SP-2358, Acton, USA) coupled via a multimode fiber to a liquid nitrogen-cooled charge coupled device camera (1340 x 100 pixels, Princeton Instruments, USA). The results show that the spectral range of the AuNRs TPL is from 400 nm to 650 nm and the TPEF emission spectrum of the RB is insignificant under the present excitation condition. This result indicates that the TPL image of the AuNRs with longitudinal plasmon resonance of 850 nm

could be obtained by using the excitation wavelength which matches the longitudinal plasmon resonance of AuNRs.

Herein, the QWP was also adopted after the linear polarizer. The fabrication laser power of 0.75 mW with circular polarization at the optimal fabrication wavelength of 715 nm was used (RB concentration 5.0 mM). Due to the generation of highly efficient TPL, the AuNRs can be attractive contrast agents for imaging 3D fabricated microstructures. Therefore, we examined the tomographic profile of the fabricated AuNRs filled microstructure by TPL imaging. Figure 5(a) shows the TPL image of a fabricated 3D, AuNRs-doped, woodpile-like BSA microstructure filled with AuNRs. The two-layer structure has a base area of $24 \times 24 \mu\text{m}^2$ and a height of $4 \mu\text{m}$. The width and thickness of BSA sticks are both $2 \mu\text{m}$ and the distance between the edges of adjacent sticks is $2 \mu\text{m}$. In this study, TPL 3D images were excited by the use of 0.13 mW, 100 fs laser at 850 nm and a scan rate of 50 kHz. Figure 5(b) is the 2D bright-field image of the woodpile-like microstructure (Fig. 5(a)). The SEM zoom in image (Fig. 5(c)) shows clear and intact AuNRs inside the crosslinked BSA. These results indicate that there was no change to the morphology of the AuNRs after the fs laser fabrication process when 0.75 mW fabrication laser power was implemented. Therefore, crosslinked protein microstructures filled with intact AuNRs can be fabricated by using lower laser power through plasmonic enhancement. This approach not only can create the freeform 3D crosslinked protein microstructure, but also avoid the use of a high fabrication laser power to damage the AuNRs. Moreover, the BSA with AuNRs material is biocompatible, and therefore ready for bioapplications such as 3D scaffolds to cues for cell binding.

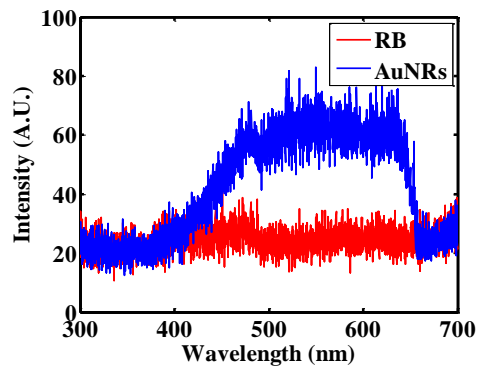


Fig. 4. TPEF and TPL spectra of RB and AuNR solutions, respectively.

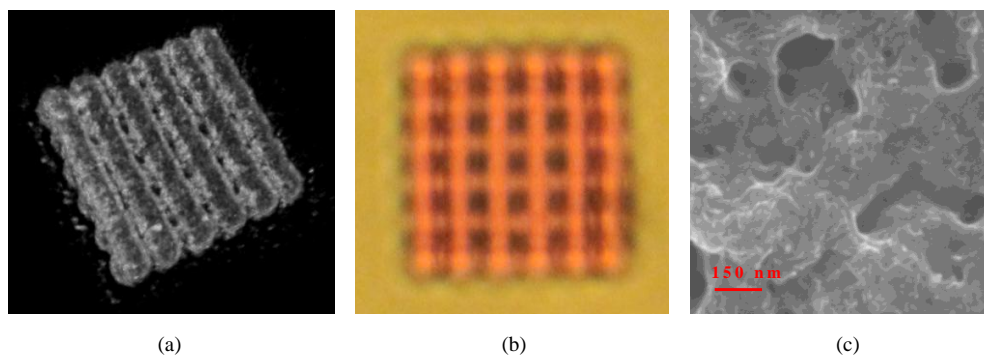


Fig. 5. An AuNRs-doped 3D woodpile BSA microstructure imaged with (a) 3D TPL, (b) 2D bright field, and (c) SEM.

4. Conclusions

The 3D crosslinked BSA microstructure filled with AuNRs was fabricated by using TPC processing. To avoid AuNRs damage in the 3D crosslinked BSA microstructures, the laser wavelength was first chosen as 715 nm for the RB TPA, but not for the AuNRs with longitudinal plasmon resonance of 850 nm. Moreover, with the plasmonic assistances of AuNRs for two-photon excitation of RB to enhance the BSA TPC efficiency, the fabrication laser power was reduced. As a result, 3D BSA microstructures remained with AuNRs can be successfully fabricated at the laser power below 0.8 mW. The approach described in this work can be used to manufacture 3-D, AuNRs-doped, protein microstructures with the desired plasmonic properties for crosslinking, TPL imaging, and photothermal therapy applications.

Acknowledgments

This work was supported by the National Research Program for Genomic Medicine (NRPGM) of the National Science Council (NSC) in Taiwan (NSC 97-3112-B-006-013) and (NSC 97-3111-B-006-004).